Conformational Studies on 2′,3′-Unsaturated Pentopyranosyl Nucleosides by ^{1}H NMR Spectroscopy. Impact of $\pi \rightarrow \sigma^*$ Interactions on the Axial Preference of the Purine versus Pyrimidine Nucleobase

Matjaž Polak,[†] Bogdan Doboszewski,[‡] Piet Herdewijn,[‡] and Janez Plavec*,[†]

Contribution from the National Institute of Chemistry, Hajdrihova 19, SI-1115 Ljubljana, Slovenia, and Laboratory of Medicinal Research, Rega Institute, Katholieke Universiteit Leuven, Minderbroedersstraat 10, B-3000 Leuven, Belgium

Received October 23, 1996. Revised Manuscript Received June 19, 1997[⊗]

Abstract: A variable-temperature ^{1}H NMR study on β- and α-D-*glycero*-pent-2′-enopyranosyl nucleosides **1**−**10** has shown that the constituent pyranosyl moiety is involved in a rapid two-state $^6H_5 \rightleftarrows {}^5E/{}^5S_4$ conformational equilibrium. The results of the conformational analysis of $^3J_{HH}$ coupling constants were compared with the trends of X-ray crystallography and *ab initio* calculations, which support the two-state dynamic equilibrium and suggest that the equilibrium is affected by the nature of the heterocyclic aglycon. The β nucleosides **1**−**5** adopt predominantly (approximately 95% in purine and 80% in pyrimidine nucleosides at 298 K) the conformation that is intermediate between the ^5E and $^5S_4$ canonical forms, where both the nucleobase and 4′-OH are in the axial orientation. The pyranosyl moiety of α-purine nucleosides **6** and **7** is involved in an unbiased two-state conformational equilibrium. On the other hand, the α-pyrimidine nucleosides **8**−**10** show a conformational bias of ca. 75% toward ^5E canonical form. The van't Hoff type analysis of the changes in the conformational equilibrium with temperature afforded thermodynamic data on $^6H_5 \rightleftarrows {}^5E/{}^5S_4$ conformational equilibrium in **1**−**10**. The comparative analysis of $\Delta H°$ has shown that $^6H_5 \rightleftarrows {}^5E/{}^5S_4$ conformational equilibrium in **1**−**10** is driven by the fine tuning of O6′−C1′−N1/9 anomeric effect, the gauche effect of the [O6′−C5′−C4′−O4′] fragment, the interaction between π-system of the C2′−C3′ bond with the heterocyclic aglycon and 4′-OH in the allylic position, and the intrinsic steric effect. Dissection of the individual contributions to the drive of conformational equilibrium of **1**−**10** has shown that the relative strength of $\pi \rightarrow \sigma^*_{C1'-N1/9}$ interactions in purine *vs* pyrimidine nucleobases increases in the following order: cytosine < uracil < thymine < adenine < guanine.

Introduction

The anomeric and gauche effects are well recognized as important factors in defining the predominant conformational state of the sugar moiety in nucleosid(t)es[1,2] and many other heteroatom-contaning (cyclic) systems.[3] Anomeric effect has been introduced in carbohydrate chemistry, where alkoxy and halogen substituents at the anomeric carbon atom of pyranosides show a tendency to occupy the axial position.[3,4] The origin of the anomeric effect can be explained in terms of electrostatic interactions[4,5] or orbital overlap[6] and is still a matter of debate. Anomeric effect in natural pentofuranosyl nucleosides drives North ⇄ South equilibrium toward North, where the nucleobase is in the pseudoaxial orientation, and one of the O4′ lone pairs is in antiperiplanar orientation with respect to the glycosyl bond.[1,2] There are few consequences of the O−C−N anomeric effect. These are (1) an axial preference of the aglycon in order to provide optimum geometry for orbital interaction which is opposed by steric repulsions, (2) a shortening of O4′−C1′ and lengthening of C1′−N bond due to the population of an antibonding orbital, and (3) a widening of the O−C−N angle when base is in axial orientation and closure of O−C−N angle to values smaller than tetrahedral when base is in equatorial orientation.[7]

The gauche effect is the preference for gauche conformations rather than trans in systems like X−C−C−Y, where X and Y are electronegative atoms or groups.[8,9] It has been shown that 3′-OH and 3′-phosphate in 2′-deoxynucleos(t)ides drive the North ⇄ South pseudorotational equilibrium in aqueous solution toward South where [O4′−C4′−C3′−OH(OPO$_3$H$^-$)] fragment is in gauche orientation.[2] The vinylogous anomeric effect[10−12] was introduced to explain the axial orientations in α-chloro ketoximes.[10] Similar observations were made much earlier by Corey, who has found that the halogen in 2-halocyclohexanones

* Author to whom correspondence should be addressed: email janez.plavec@ki.si.
† National Institute of Chemistry.
‡ Rega Institute.
⊗ Abstract published in *Advance ACS Abstracts,* September 15, 1997.
(1) Saenger, W. *Principles of Nucleic Acid Structure*; Springer-Verlag: New York, 1984.
(2) Plavec, J.; Tong, W.; Chattopadhyaya, J. *J. Am. Chem. Soc.* **1993**, *115*, 9734−9746.
(3) (a) Kirby, A. J.; Williams, N. H. *The Anomeric Effect and Associated Stereoelectronic Effects*; American Chemical Society: Washington, DC, 1993; pp 55−96. (b) Juaristi, E.; Cuevas, G. *Tetrahedron* **1992**, *48*, 5019−5087. (c) Tvaroška, I.; Bleha, T. In *Advances in Carbohydrate Chemistry and Biochemistry*; Tipson, R. S., Horton, D., Eds.; Academic Press: San Diego, CA, 1989; Vol. 47, pp 45−123.
(4) Edward, J. T. *Chem. Ind.* **1966**, 1102−1104.
(5) (a) Eliel, E. L.; Giza, C. A. *J. Org. Chem.* **1968**, *33*, 3754−3758. (b) Hutchins, R. O.; Kopp, L. D.; Eliel, E. L. *J. Am. Chem. Soc.* **1968**, *90*, 7174−7175.
(6) Romers, C.; Altona, C.; Buys, H. R.; Havinga, E. *Top. Stereochem.* **1969**, *4*, 39−97.
(7) Lo, A.; Shefter, E.; Cochran, T. G. *J. Pharm. Sci.* **1975**, *64*, 1707−1710.
(8) Wolfe, S. *Acc. Chem. Res.* **1972**, *5*, 102−111.
(9) Phillips, L.; Wray, V. *J. Chem. Soc., Chem. Commun.* **1973**, 90−91.
(10) (a) Denmark, S. E.; Dappen, M. S.; Sear, N. L.; Jacobs, R. T. *J. Am. Chem. Soc.* **1990**, *112*, 3466−3474. (b) Denmark, S. E.; Dappen, M. S. *J. Org. Chem.* **1984**, *49*, 798−806.
(11) Kovacs, L. *Bull. Soc. Chim. Fr.* **1995**, *132*, 1015−1019.
(12) Zefirov, N. S. *Tetrahedron* **1977**, *33*, 3193−3202.

S0002-7863(96)03683-9 CCC: $14.00

is mainly in the axial position.[13] The generalized anomeric effect has been extended to transition states to rationalize stereochemical discrimination. The kinetic anomeric effect is used to explain the relative rates of departure of leaving groups and various kinetic data. In the study[14] of substituent effect on the rate of Claissen rearrangement, it was suggested that rate acceleration is a chemical consequence of kinetic vinylogous anomeric effect.

Carbohydrate modifications of nucleosides offer an approach to modify the biological activity of a nucleoside, and it has led to a series of antivirial and antitumoral drugs. The carbohydrate modifications likewise offers opportunities to obtain new antisense constituents, which are stable against nuclease degradation and show favorable hydrolization properties.[15] D-*Glycero*-pent-2′-enopyranosyl nucleosides **1**−**10** are starting materials for the introduction of the 3′-hydroxymethyl appendix, and after the inversion of configuration at the 4′-position, one obtains nucleoside analogues for antisense and antiviral studies. These compounds can also be considered as model compounds to begin studying the conformational behavior of more complex nucleosides with an unsaturated six-membered carbohydrate moiety.[15c]

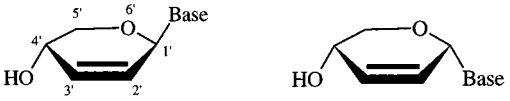

1 - 5 **6 - 10**

1 (βA), **6** (αA) : Base = adenin-9-yl
2 (βG), **7** (αG) : Base = N^2-isobutyrylguanin-9-yl
3 (βC), **8** (αC) : Base = cytosin-9-yl
4 (βT), **9** (αT) : Base = thymin-9-yl
5 (βU), **10** (αU) : Base = uracil-9-yl

Since the nucleobases in **1**−**10** occupy both anomeric and allylic positions, we have initiated conformational study of their constituent pyranosyl moieties by the combination of NMR spectroscopy, X-ray crystallography, and *ab initio* calculations in order to gain a deeper insight into the predominant forces which drive their conformational equilibrium. X-ray crystal structures of three of the compounds (**1**−**3**) were published earlier together with the preliminary report on the conformation in DMSO solution.[15a] The variability in the puckering of the pyranosyl moiety observed in the X-ray crystal structures of **1**−**3** suggests that the conformation of the unsaturated pyranosyl nucleosides is partially controlled by the purine *vs* pyrimidine nature of the heterocycle linked to the C1′ of the carbohydrate moiety (*i.e.* anomeric center). However, a noticeable difference between the solution state conformation and the solid state conformation can be expected. The crystal-packing forces additionally determine the conformation through the hydrogen-bonding and base-stacking forces between bases.[1]

Interpretation of the experimental proton−proton coupling constants ($^3J_{HH}$) suggests that the pyranosyl moiety in **1**−**10** is involved in a two-state equilibrium. The assumed two-state conformational equilibrium is in agreement with the *ab initio* calculations *in vacuo*. The variation of $^3J_{HH}$ with the change of temperature and solvent gives us thermodynamic data on the conformational equilibrium in **1**−**10** and therefore enables insight into the interplay of stereoelectronic effects. From the geometric considerations based on the model building of the structures of **1**−**10**, it is apparent that the (solution state) conformation will be determined by the competing anomeric effect of the nucleobase, gauche effect of 4′-OH with O6′, the interaction of the π-system along C2′−C3′ with both the heterocyclic aglycon and 4′-OH in allylic positions, and the inherent steric effects. We have initiated conformational studies with the following objectives in mind: (1) to describe the conformational equilibrium of **1**−**10** in solution and to determine the enthalpy and entropy contributions to the drive of the equilibrium, (2) to establish if there is any nucleobase-dependent interaction of the π-system with the heterocyclic moiety (purine *vs* pyrimidine) and how it drives the pyranosyl conformation of **1**−**10** and (3) to evaluate in the thermodynamic terms $\pi \rightarrow \sigma^*_{C1'-N9/1}$ interaction in the modified nucleosides for the first time.

Procedures

The conformation of the pyranose ring was analyzed on the basis of the vicinal proton−proton coupling constants $^3J_{4'5'}$, $^3J_{4'5''}$, $^3J_{1'2'}$, and $^3J_{3'4'}$. This analysis depends on three essential translational steps: (1) proton−proton coupling constants are translated into proton−proton torsion angles (Φ_{HH}), (2) Φ_{HH} are translated into the corresponding endocyclic torsion angles (ν_i), and (3) ν_i are translated into the puckering parameters describing geometry of the pyranose ring. All three steps were incorporated into the computer program PYRLW (see the Experimental Section).

The first translational step is done with the use of the generalized Karplus equations. In our conformational analysis, we utilized two separate Karplus equations for coupling constants along Csp^3-Csp^3 and Csp^2-Csp^3 bonds, which differ greatly in their elaboration and quality.

A. C4′−C5′ Torsion. The generalized Karplus equation (eq 1), which was introduced by Altona *et al.*,[16] correlates the $^3J_{HH}$ coupling constant and the torsion angle between the coupled atoms (Φ_{HH}). Additionally, eq 1 includes terms which correct for the electronegativity and the relative position of the substituents along the coupling path.[16]

$$^3J_{HH} = P_1 \cos^2 \Phi_{HH} + P_2 \cos \Phi_{HH} + P_3 + \sum_{i=1}^{4} \lambda_i \{P_4 + P_5 \cos^2(\zeta_i \Phi_{HH} + P_6 |\lambda_i|)\} \quad (1)$$

where P_1 to P_6 are empirically determined parameters,[16a] λ_i is empirical group electronegativity, and ζ_i denotes the relative orientation of substituents.[16]

B. C1′−C2′ and C3′−C4′ Torsions. The simple two-parameter Karplus equation described by Garbisch[17] has been used to translate the experimental $^3J_{HH}$ into proton−proton torsion angles across Csp^2-Csp^3 fragments. It should be noted

(13) (a) Corey, E. J. *J. Am. Chem. Soc.* **1953**, *75*, 2301−2304. (b) *Ibid.* **1953**, *75*, 3297−3299.

(14) (a) Curran, D. P.; Suh, Y. G. *J. Am. Chem. Soc.* **1984**, *106*, 5002−5004. (b) Coates, R. M.; Rogers, B. D.; Hobbs, S. J.; Peck, D. R.; Curran, D. P. *J. Am. Chem. Soc.* **1987**, *109*, 1160−1170.

(15) (a) Doboszewski, B.; Blaton, N.; Herdewijn, P. *J. Org. Chem.* **1995**, *60*, 7909−7919. (b) Doboszewski, B.; De Winter, H.; Van Aerschot, A.; Herdewijn, P. *Tetrahedron* **1995**, *51*, 12319−12336. (c) Luyten, I.; Herdewijn, P. *Tetrahedron* **1996**, *52*, 9249−9262. (d) Doboszewski, B.; Blaton, N.; Herdewijn, P. *Tetrahedron Lett.* **1995**, *36*, 1321−1324. (e) Doboszewski, B.; Blaton, N.; Rozenski, J.; De Bruyn, A.; Herdewijn, P. *Tetrahedron* **1995**, *51*, 5381−5396. (f) Herdewijn, P.; De Winter, H.; Doboszewski, P.; Verheggen, I.; Augustyns, K.; Hendrix, C.; Saison-Behmoars, T.; De Ranter, C.; Van Aerschot, A. In *Carbohydrate Modifications in Antisense Research*; ACS Symposium Series 580; Sanghvi, Y. S., Cook, P. D., Eds.; American Chemical Society: Washington, DC, 1994; Chapter 6, pp 80−99. (g) Doboszewski, B.; Herdewijn, P. *Tetrahedron* **1996**, *52*, 1651−1668. (h) Doboszewski, B.; Herdewijn, P. *Nucleosides Nucleotides* **1996**, *15*, 1495−1518.

(16) (a) Altona, C.; Francke, R.; de Haan, R.; Ippel, J. H.; Daalmans, G. J.; Hoekzema, A. J. A. W.; van Wijk, J. *Magn. Reson. Chem.* **1994**, *32*, 670. (b) Haasnoot, C. A. G.; de Leeuw, F. A. A. M.; Altona, C. *Tetrahedron* **1980**, *36*, 2783−2792.

(17) (a) Garbisch, E. W. *J. Am. Chem. Soc.* **1964**, *86*, 5561−5564. (b) $^3J_{HH} = 6.6 \cos^2 \Phi + 2.6 \sin^2 \Phi$.

however, that the parametrization is of qualitative nature and discrepancies between the calculated and experimental coupling constants of up to 1 Hz are expected.

C. C2′−C3′ Torsion. An additional piece of the information concerning the conformation of pyrano moiety comes from the structures of **1**−**10**, namely, the parts across C2′−C3′ that are expected to be planar, *i.e.*, ν_2[C1′−C2′−C3′−C4′] = 0°. We have incorporated this fact in our optimization routine by applying a strong penalty if ν_2 deviates from zero.

The second step in our conformational analysis is defined by the relationships between exocyclic proton−proton torsion angles (Φ_{HH}) and the corresponding endocyclic torsion angles (ν_i) which are given as a set of simple linear equations:

$$\Phi_{HH}^{\ exo} = A\nu_i^{endo} + B \qquad (2)$$

Note that each pair of vicinal ring protons has its own parameters, *A* and *B*. For the situation where all bond distances are equal and all valence angles between ring atoms are equal, which would give rise to ideal Newman projections, $A = 1$ and $B = 0°$ for cisoid exocyclic protons and $B = \pm 120°$ for transoid exocyclic protons along Csp^3-Csp^3 bond. However, the variation in valence angles for realistic six-membered rings in **1**−**10** causes a considerable deviation from the ideal projection symmetry. We have turned to *ab initio* calculations on compounds with both β- and α-configurations to obtain *A*, *B* parameter sets in eq 2. Several completely free geometry optimizations at HF/3-21G and HF/6-31G** levels were performed on the structures of βA (**1**), βG (**2**), βC (**3**), αA (**6**), and αC (**8**). The four proton−proton torsion angles $\Phi_{1'2'}$, $\Phi_{3'4'}$, $\Phi_{4'5'}$, and $\Phi_{4'5''}$ and the corresponding endocyclic torsion angles ν_1, ν_3, and ν_4 were extracted from the optimized structures of β-anomers (Figure 1) and α-anomers (Figure 2) and used to calculate the *A* and *B* parameters in eq 2. We have noticed that the *A* and *B* parameters for βA (**1**) and βC (**3**), as well as for αA (**6**) and αC (**8**) are indeed very similar and therefore no separate sets of *A* and *B* parameters for purine and pyrimidine nucleosides were used. The results of the parametrizations of eq 2 are given in Table 1.

The third translational step in our conformational analysis is the calculation of the puckering parameters from the set of endocyclic torsion angles with the truncated Fourier formalism. According to truncated Fourier formalism,[18] the endocyclic torsion angles (ν_i)[19] are interrelated and defined by the puckering parameters P_2, Φ_2, and Φ_3 according to eq 3.

$$\nu_i = \Phi_2 \cos(P_2 + 4\pi i/6) + \Phi_3 \cos(\pi i) \qquad (3)$$

The puckering coordinates Φ_2, P_2, and Φ_3 define the conformation of a given six-membered ring as a single point in a cylindrical conformational space.[18] They can be replaced by a spherical polar set P_2, *Q*, and Θ, where *Q* is the total puckering amplitude

$$Q = \sqrt{\Phi_2^2 + \Phi_3^2} \qquad (4)$$

and

$$\Theta = \arctan(\Phi_2/\Phi_3) \qquad (5)$$

The simplified two-dimensional projection of a sphere for a particular value of puckering amplitude *Q* is shown in Figure 3. The center of the projection at Θ = 0° corresponds to a canonical $^1C_4$ form. Other typical canonical forms occur at the specific points on the projection circles with distinctive P_2 values (labeled by filled dots in Figure 3). Half-chairs (H) are characterized[18] by Θ = ±45° and $P_2 = n(60°)$, envelopes (E) are by Θ = ±49.1° and $P_2 = 30° + n(60°)$, and screw-boats (S) are by Θ = ±63.4° and $P_2 = n(60°)$ ($n = 0-5$).

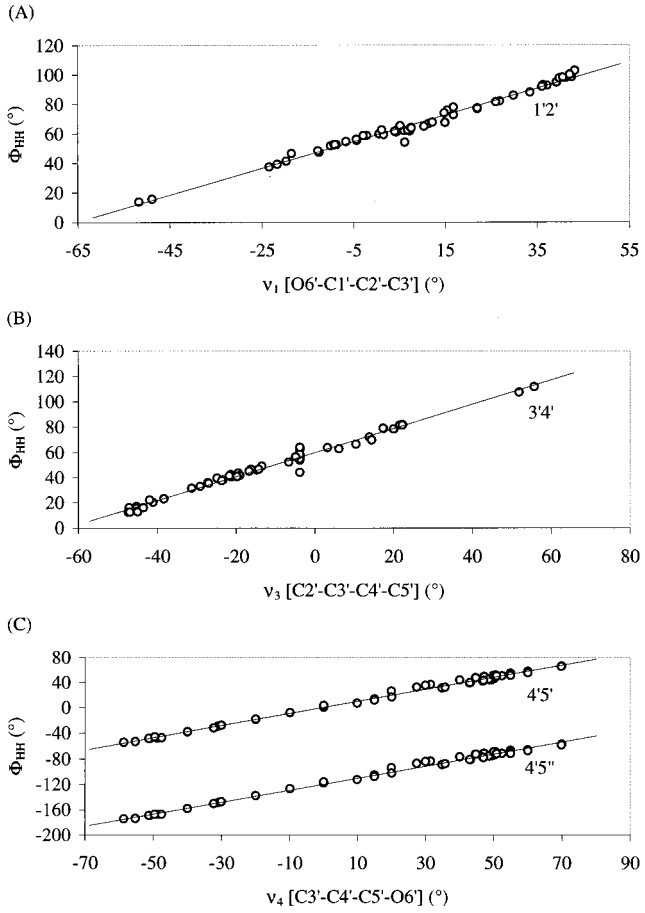

Figure 1. The correlation between proton−proton (Φ_{HH}) and the corresponding endocyclic (ν_i) torsion angles along C1′−C2′ (panel A), C3′−C4′ (panel B), and C4′−C5′ bonds (panel C) for β nucleosides **1**−**5**. 64 data points originate from *ab initio* optimized geometries of βA (**1**), βG (**2**), and βC (**3**) with 3-21G and 6-31G** basis sets. Straight lines were obtained with the linear regression analysis according to the relation $\Phi_{HH} = A\nu_i + B$. *A* and *B* values are given in Table 1.

The observed coupling constants are time-averaged and therefore $J^{expt} = \sum_i x^i J^i$, where x^i is a mole fraction of a particular conformer and J^i is the respective limiting coupling constant. In our analysis of the experimental coupling constants, we have assumed a two-state conformational equilibrium based on *ab initio* profile calculations (*vide infra*). Therefore, the $^3J_{HH}$ coupling constants can be calculated from a given geometry of the two conformers and their respective mole fractions with the use of eq 6.

$$J^{calcd} = x^I J^I(P_2^{\ I}, \Phi_2^{\ I}, \Phi_3^{\ I}) + x^{II} J^{II}(P_2^{\ II}, \Phi_2^{\ II}, \Phi_3^{\ II}) \qquad (6)$$

The problem of the conformational analysis of pyranosyl moiety in **1**−**10** is to find seven independent parameters (P_2, Φ_2, and Φ_3 for the two conformers and the mole fraction, see eq 6) which best fit the set of four experimental $^3J_{4'5'}$, $^3J_{4'5''}$, $^3J_{1'2'}$, and $^3J_{3'4'}$ coupling constants. Another known parameter is that the endocyclic torsion ν_2 is 0° because the fragment along C2′−C3′ double bond has to be planar. Since the number of unknowns is larger than the number of available $^3J_{HH}$ at a

(18) (a) Haasnoot, C. A. G. *J. Am. Chem. Soc.* **1993**, *115*, 1460−1468. (b) Haasnoot, C. A. G. *J. Am. Chem. Soc.* **1992**, *114*, 882−887.

(19) The endocyclic torsion angles are defined as follows: ν_0 [C5′−O6′−C1′−C2′], ν_1 [O6′−C1′−C2′−C3′], ν_2 [C1′−C2′−C3′−C4′], ν_3 [C2′−C3′−C4′−C5′], ν_4 [C3′−C4′−C5′−O6′], and ν_5 [C4′−C5′−O6′−C1′].

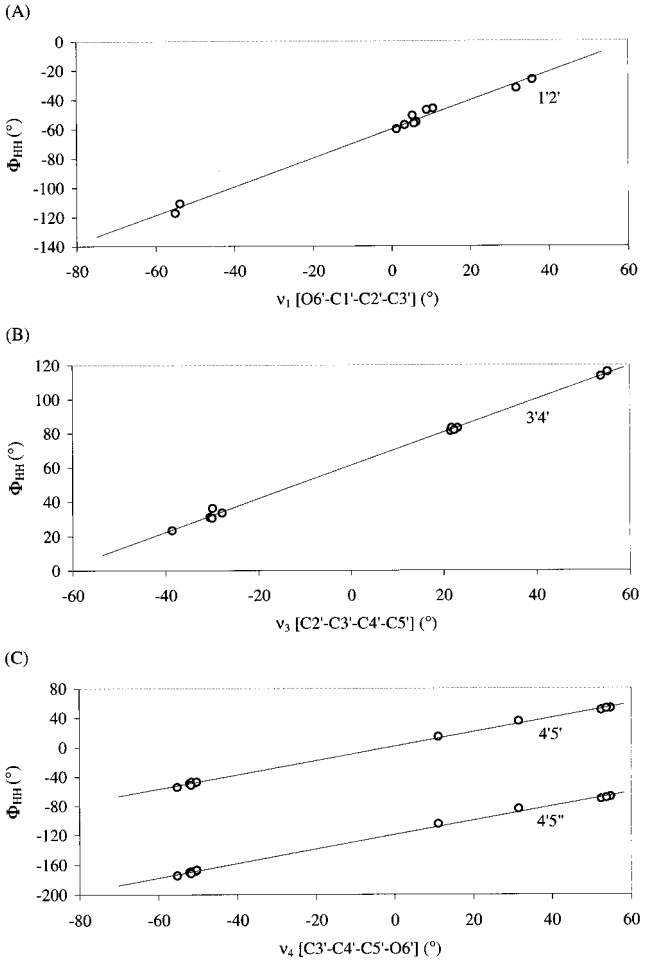

Figure 2. The correlation between proton−proton (Φ_{HH}) and the corresponding endocyclic (ν_i) torsion angles along C1′−C2′ (panel A), C3′−C4′ (panel B), and C4′−C5′ bonds (panel C) for α nucleosides **6**−**10**. Eleven data points originate from *ab initio* optimized geometries of αA (**6**) and αC (**8**) with 3-21G and 6-31G** basis sets. Straight lines were obtained with the linear regression analysis according to the relation $\Phi_{HH} = A\nu_i + B$. *A* and *B* values are given in Table 1.

particular temperature, the assumption is made that the geometry of the pyranose ring in the conformational equilibrium remains constant and only the population changes with the change of temperature or solvent. The iterative least-squares optimization procedure has been used to find the best fit of the experimental and the calculated $^3J_{HH}$. During this iterative procedure, the conformational space of the pyranosyl moiety has been thoroughly examined by performing optimizations from several starting geometries (see the Experimental Section for details).

Results

The conformational analysis of **1**−**10**[20] is based on the interpretation of proton−proton coupling constants (J_{HH}) which have been extracted from ^{1}H NMR spectra acquired at 300 MHz in D_2O in the temperature range from 278 to 358 K in 20 K steps (data at two limiting temperatures are given in Table 2, whereas data at 298, 318, and 328 K are not shown but were used in the analysis) and in DMSO-d_6 at 298 K (Table 2). Qualitative analysis of $^4J_{1'3'}$ and $^4J_{2'4'}$ shows that the deviation from the plane defined by C2′−C3′ is bigger for H1′ than for H4′ which suggests[21] that the predominant conformer in **1**−**10** is characterized by ^{5}E puckering (*vide infra*). In the ^{5}E canonical form, H1′ is axial, whereas H4′ is equatorial, consistent with the higher $^4J_{1'3'}$ in comparison with $^4J_{2'4'}$ experimental coupling constants (Table 2). Note that the relative ratio between the experimental $^4J_{1'3'}$ and $^4J_{2'4'}$ coupling constants is approximately two in all compounds, except in αA (**6**) and αG (**7**), which suggests their lower conformational purity (Table 2).

The X-ray crystal structures of **1**−**3** are known.[15a] The relevant puckering coordinates for the pyranosyl moieties of the two independent structures in the unit cells of **1**−**3** are given in Table 3. It turns out that both X-ray crystal structures of purine nucleosides βA (**1**) and βG (**2**) show similar conformations that are intermediate between $^5H_6$ half-chair and ^{5}E and E_6 envelope forms, respectively, whereas βC (**3**) is characterized by $^6H_5$ puckering (Table 3 and Figure 3). Our first step in the conformational analysis was to determine if **1**−**3** adopt similar conformations in aqueous solution as they do in the solid state. We have extracted $\Phi_{1'2'}$, $\Phi_{3'4'}$, $\Phi_{4'5'}$, and $\Phi_{4'5''}$ proton−proton torsion angles from the X-ray crystal structures of βA (**1**), βG (**2**), and βC (**3**) and used them to calculate the corresponding vicinal proton−proton coupling constants (Table 3). The comparison of the calculated and the experimental $^3J_{HH}$ at 298 K in D_2O has shown that the agreement is more or less acceptable for βA (**1**). The biggest difference between the calculated and the experimental $^3J_{HH}$ coupling constants in βA (**1**) is 1.0 Hz for $J_{4'5''}$ (Table 3). This suggests that the conformation adopted by the pyranosyl moiety of βA (**1**) in X-ray crystal structure and in D_2O are very similar. The agreement between the calculated and the experimental $^3J_{HH}$ is worse for βG (**2**) with the largest discrepancy of 3.3 Hz for $J_{4'5'}$ (Table 3). This means that the proton−proton torsion angles found in the X-ray crystal structure of βG (**2**) cannot adequately account for the experimental $^3J_{HH}$ coupling constants at 298 K. The difference between the calculated and the experimental $^3J_{HH}$ at 298 K for βC (**3**) is as high as 7.2 Hz for $^3J_{4'5''}$ which clearly shows that the (predominant) conformation in solution differs enormously from the conformation found in the X-ray crystal structure of βC (**3**).

Subsequently, we have performed the optimization of the geometry of the puckered pyranosyl moiety in **1**−**3** in order to find the best fit of the experimental and the calculated $^3J_{HH}$ at 298 K in D_2O in terms of a single-state conformation. These analyses of the experimental $^3J_{4'5'}$, $^3J_{4'5''}$, $^3J_{1'2'}$, and $^3J_{3'4'}$ coupling constants at 298 K in **1**−**3** resulted in ΔJ values below 0.8 Hz for βA (**1**), 0.4 Hz for βG (**2**), and 2.1 Hz for βC (**3**) (Table 3). The optimized geometries of the assumed single-state conformers of **1**−**3** are very similar and close to ^{5}E canonical form, which is close to the conformation found in the X-ray crystal structure of βA (**1**), but show much poorer agreement with $^3J^{expt}$ than the two-state model (*vide infra*). The optimized geometry of βC (**3**) is very different from the puckering found in its X-ray crystal structure (Table 3). The analysis of the experimental $^3J_{HH}$ coupling constants at 298 K in **1**−**3** in terms of a single-state conformation results in individual differences between experimental and calculated $^3J_{HH}$ of up to 2.1 Hz (Table 3). This indicates a serious error in the assumption of a single-state model comparing to the two-state model in terms of agreement of the observed and calculated $^3J_{HH}$ coupling

(20) The configuration at the anomeric center in **1**−**10** has been independently established[15a] by 1D difference NOE measurements. Nucleosides **1**−**5** exhibit H1′ ↔ H5″ and H8/6 ↔ H5′ NOE interactions which unequivocally proves their β-configuration. All α-analogues **6**−**10** exhibit NOE contacts between H1′ ↔ H4′, H1′ ↔ H5′, and H8/6 ↔ H5″, which proves that H1′, H4′, and H5′ protons are on the β face of the sugar moiety in **6**−**10** and the α-configuration at the anomeric center. In addition, the NOE interactions between H3′ and H6 in pyrimidine and between H3′ and H8 in purine nucleosides were observed which show that the base adopts predominantly *anti* conformation in **1**−**10**.

(21) Jackman, L. M.; Sternhell, S. *Applications of Nuclear Magnetic Resonance Spectroscopy in Organic Chemistry*; Pergamon: London, 1969; pp 315−341.

Table 1. The *A* and *B* Parameters which Relate Proton−Proton Torsion Angles to Endocyclic Torsion angles (eq 2)

C1′ configuration	*A* or *B*	$\Phi_{1'2'}$	$\Phi_{3'4'}$	$\Phi_{4'5'}$	$\Phi_{4'5''}$
β[a]	*A*	0.892	0.952	0.961	0.965
	B	58.368°	60.620°	0.967°	−119.430°
α[b]	*A*	0.975	0.971	0.974	0.976
	B	−60.268°	61.188°	1.334°	−119.271°

[a] The A and B parameters were calculated with the linear regression based on the set of 64 sets of exocyclic proton−proton torsion angles (Φ_{HH}) and endocyclic torsion angles (ν_i) from *ab initio* HF/3-21G- and HF/6-31G**-optimized geometries of βA (**1**), βG (**2**), and βC (**3**). The following Pearson correlation coefficients were found: 0.997 ($\Phi_{1'2'}$), 0.998 ($\Phi_{3'4'}$), 0.998 ($\Phi_{4'5'}$), and 0.998 ($\Phi_{4'5''}$). [b] A set of 11 Φ_{HH} and ν_i torsion angles from HF/3-21G-optimized geometries of αA (**6**) and αC (**8**) was used to calculate *A* and *B* parameters. The Pearson correlation coefficients are 0.995 ($\Phi_{1'2'}$), 0.999 ($\Phi_{3'4'}$), 0.999 ($\Phi_{4'5'}$), and 0.999 ($\Phi_{4'5''}$).

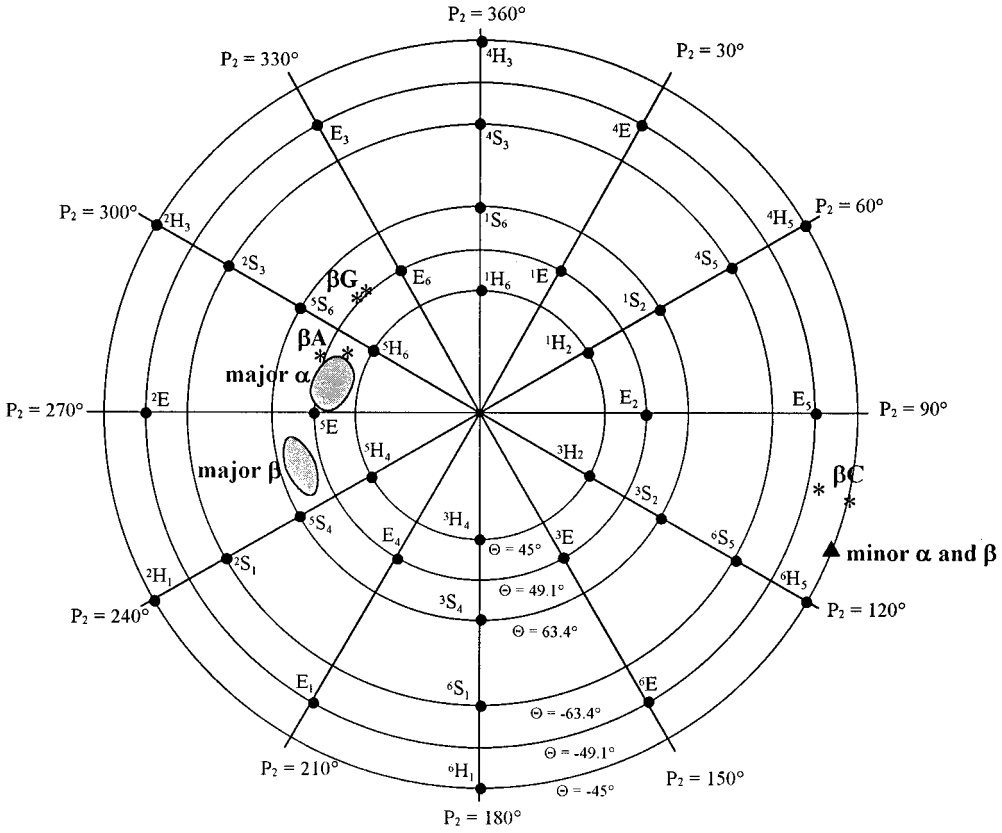

Figure 3. Schematic polar projection of the sphere showing the conformational space accessible to the pyranosyl moieties in **1**−**10**. For clarity, only the projection circles for the envelope ($\Theta = \pm 45°$), half-chair ($\Theta = \pm 49.1°$), and screw-boat ($\Theta = \pm 63.4°$) canonical forms, which are characteristic for the puckering of pyranosyl moieties in **1**−**10**, are shown. Shaded areas represent part of conformational space that is characteristic for the puckering of the major conformer in β-anomers **1**−**5** and in α-anomers **6**−**10**. The geometry of the minor conformer, which was kept fixed during the iterative optimization procedure of experimental $^3J_{HH}$, is shown by a filled triangle. The geometries of the X-ray crystal structures[15a] of βA (**1**), βG (**2**), and βC (**3**) are shown by asterisks. Note that **1**−**3** have crystallized with the two structures in the unit cell (Table 3).[15a]

constants. Additionally, all of the vicinal coupling constants change with the change of temperature from 278 to 358 K (see Table 2). This clearly indicates that no single conformer is consistent with the complete set of 24 temperature- and solvent-dependent $^3J_{HH}$ coupling constants for a particular nucleoside (**1**−**10**).

To examine the feasibility of a two-state conformational equilibrium, we have performed several *ab initio* optimizations on **1**−**10** *in vacuo* at the HF/3-21G and HF/6-31G** levels. The energy profiles on βA (**1**) and βC (**3**) at the HF/3-21G level have shown two energy wells that are separated with the barrier of 34.5 and 45.2 kJ mol^{-1}, respectively (see Figure 4). The heights of the barriers suggest a rapid exchange on the NMR time scale between interconverting conformers, which results in the time-averaged coupling constants and chemical shifts of **1**−**10**. The energy minimization of **1**−**3**, where all degrees of freedom were freely optimized, resulted in the two lowest energy conformers for **1**−**3**, which are given in Table 3. The energy difference between the two minima is small and suggests that both conformations are possible. The lowest energy conformers for βA (**1**) and βG (**2**) are characterized by very similar puckering, which is very close to $^5H_6$ canonical form and closely resembles the conformations found in the X-ray crystal structures of βA (**1**) and βG (**2**) (Table 3). The conformations of βA (**1**) and βG (**2**) that best fit the experimental $^3J_{HH}$ at 298 K with the assumption of a single-state model are also similar to the conformers in the HF/3-21G lowest energy $^5E/^5H_6$ conformational pool for βA (**1**) (Table 3 and Figure 4). The puckering of the second lowest energy conformers in βA (**1**) and βG (**2**) is close to $^6H_5$ canonical form. The energetic preference at the HF/3-21G level for $^5H_6$ over $^6H_5$ conformation is 2.2 kJ mol^{-1} in βA (**1**) and 8.0 kJ mol^{-1} in βG (**2**), which is in qualitative agreement with the results of our evaluation of the energetics of the assumed two-state conformational equilibrium in βA (**1**) and βG (**2**) (*vide infra*). For βC (**3**), the geometry of the X-ray crystal structure is very similar to the geometry of the lowest energy conformer at the HF/3-21G level, both being intermediate between the $^6H_5$ and E_5 canonical forms. On the contrary, the discrepancy between the experimental (298 K) and the calculated $^3J_{4'5'}$, $^3J_{4'5''}$, $^3J_{1'2'}$, and $^3J_{3'4'}$ coupling constants based on the

Table 2. Experimental Proton−Proton Coupling Constants (J_{HH}) for **1**−**10** at Two Extreme Temperatures in D_2O and at 298 K in DMSO-d_6[a]

compd	solvent	T (K)	$^3J_{1'2'}$	$^3J_{3'4'}$	$^3J_{4'5'}$	$^3J_{4'5''}$	$^4J_{1'3'}$	$^4J_{2'4'}$	$^4J_{3'5''}$
βA (**1**)[b]	D_2O	278	3.3	5.2	2.5	1.9	1.9	0.8	0.8
		358	3.1	4.8	3.0	2.7	2.0	1.0	1.0
	DMSO	298	3.0	3.9	3.7	3.6	1.7	1.2	0.6
βG (**2**)[c]	D_2O	278	3.4	5.2	2.4	1.7	1.9	0.8	0.9
		358	3.2	5.0	2.9	2.5	1.9	1.0	1.2
	DMSO	298	2.9	4.1	3.5	3.5	1.9	1.3	0.7
βC (**3**)[d]	D_2O	278	3.1	4.5	3.2	3.2	2.0	1.1	0.9
		358	2.8	4.1	3.8	4.2	2.1	1.3	0.7
	DMSO	298	2.1	2.9	4.7	6.9	2.1		
βT (**4**)[e]	D_2O	278	3.1	4.6	3.1	3.0	2.0	1.1	0.9
		358	2.8	4.2	3.7	4.3	2.1	1.3	0.7
	DMSO	298	2.1	2.0	4.8	6.9	2.0		
βU (**5**)[f]	D_2O	278	3.2	4.7	3.1	2.8	2.0	1.1	1.0
		358	2.9	4.3	3.6	3.9	2.0	1.3	0.8
	DMSO	298	2.0	2.3	4.6	6.5	1.8	1.8	
αA (**6**)[g]	D_2O	278	2.4	3.6	4.2	5.6	1.9	1.3	
		358	2.4	3.6	4.3	5.6	1.9	1.4	
	DMSO	298	2.7	2.7	5.2	7.7	1.9	1.7	
αG (**7**)[h]	D_2O	278	2.5	3.3	4.6	6.2	1.9	1.4	
		358	2.4	3.3	4.6	6.2	1.9	1.4	
	DMSO	298	2.9	2.6	5.4	8.1	1.8	1.7	
αC (**8**)[i]	D_2O	278	1.9	4.5	3.4	3.3	2.0	1.0	0.9
		358	2.0	4.4	3.6	3.8	2.0	1.0	1.0
	DMSO	298			3.9	4.5			
αT (**9**)[j]	D_2O	278	2.0	4.4	3.4	3.6	2.0	1.0	0.9
		358	2.0	4.3	3.6	3.8	2.0	1.0	1.0
	DMSO	298	2.0	4.0	3.7	4.0	2.0	1.2	0.7
αU (**10**)[k]	D_2O	278	2.0	4.4	3.5	3.8	2.0	1.0	0.8
		358	2.1	4.2	3.7	4.1	2.0	1.1	0.9
	DMSO	298	2.0	3.9	3.9	4.7	2.0	1.3	0.5

[a] J_{HH} values (in hertz, ±0.1 Hz) have been extracted from 1D ^{1}H NMR spectra recorded at 300 MHz in D_2O in the range of 278−358 K in 20 K steps and in DMSO-d_6 at 298 K. The complete set of J_{HH} and chemical shifts in **1**−**10** at five distinct temperatures (data not shown) were simulated and iterated by the simulation module of VNMR software package. [b] δ (D_2O, 298 K, MeCN = 2.00 ppm): 8.19 (H8), 8.12 (H2), 6.49 (H3′, $^3J_{2'3'}$ = 10.2 Hz), 6.41 (H1′), 6.21 (H2′), 4.14 (H4′), 3.80 (H5′, $^2J_{5'5''}$ = 13.1 Hz), 3.75 (H5″) ppm. [c] δ (D_2O, 298 K, MeCN = 2.00 ppm): 7.99 (H8), 6.48 (H3′, $^3J_{2'3'}$ = 10.2 Hz), 6.36 (H1′), 6.18 (H2′), 4.13 (H4′), 3.83 (H5′, $^2J_{5'5''}$ = 13.0 Hz), 3.77 (H5″) ppm. [d] δ (D_2O, 298 K, MeCN = 2.00 ppm): 7.57 (H6), 6.40 (H3′, $^3J_{2'3'}$ = 10.2 Hz), 6.25 (H1′, $^5J_{1'4'}$ = 1.1 Hz), 5.90 (H5), 5.88 (H2′), 4.14 (H4′), 3.86 (H5′, $^2J_{5'5''}$ = 12.8 Hz), 3.71 (H5″) ppm. [e] δ (D_2O, 298 K, MeCN = 2.00 ppm): 7.42 (H6), 6.42 (H3′, $^3J_{2'3'}$ = 10.3 Hz), 6.23 (H1′), 5.88 (H2′), 4.16 (H4′), 3.90 (H5′, $^2J_{5'5''}$ = 12.7 Hz), 3.74 (H5″), 1.79 (CH_3) ppm. [f] δ (D_2O, 298 K, MeCN = 2.00 ppm): 7.64 (H6), 6.44 (H3′, $^3J_{2'3'}$ = 10.3 Hz), 6.24 (H1′, $^4J_{1'5'}$ = 0.3 Hz), 5.98 (H2′), 5.73 (H5), 4.14 (H4′), 3.88 (H5′, $^2J_{5'5''}$ = 12.8 Hz), 3.75 (H5″) ppm. [g] δ (D_2O, 298 K, MeCN = 2.00 ppm): 8.21 (H8), 8.18 (H2), 6.40 (H3′, $^3J_{2'3'}$ = 10.2 Hz), 6.36 (H1′, $^5J_{1'4'}$ = 1.9 Hz), 6.11 (H2′), 4.32 (H4′), 3.97 (H5′, $^2J_{5'5''}$ = 12.0 Hz), 3.62 (H5″) ppm. [h] δ (D_2O, 298 K, MeCN = 2.00 ppm): 8.09 (H8), 6.38 (H3′, $^3J_{2'3'}$ = 10.3 Hz), 6.33 (H1′, $^4J_{1'5'}$ = 0.5 Hz), 6.06 (H2′), 4.34 (H4′), 3.96 (H5′, $^2J_{5'5''}$ = 12.0 Hz), 3.61 (H5″) ppm. [i] δ (D_2O, 298 K, MeCN = 2.00 ppm): 7.63 (H6), 6.32 (H3′, $^3J_{2'3'}$ = 10.3 Hz), 6.25 (H1′, $^5J_{1'4'}$ = 2.2 Hz, $^4J_{1'5'}$ = 0.2 Hz, $^4J_{1'5''}$ = 0.3 Hz), 5.97 (H5), 5.85 (H2′), 4.17 (H4′), 3.95 (H5′, $^2J_{5'5''}$ = 12.4 Hz), 3.75 (H5″) ppm. [j] δ (D_2O, 298 K, MeCN = 2.00 ppm): 7.52 (H6), 6.34 (H3′, $^3J_{2'3'}$ = 10.3 Hz), 6.22 (H1′, $^4J_{1'5''}$ = 0.4 Hz), 5.83 (H2′), 4.18 (H4′), 3.96 (H5′, $^2J_{5'5''}$ = 12.4 Hz), 3.76 (H5″), 1.82 (CH_3) ppm. [k] δ (D_2O, 298 K, MeCN = 2.00 ppm): 7.68 (H6), 6.36 (H3′, $^3J_{2'3'}$ = 10.3 Hz, $^4J_{3'5''}$ = 0.9 Hz), 6.23 (H1′, $^4J_{1'5''}$ = 0.4 Hz), 5.84 (H2′), 5.81 (H5), 4.19 (H4′), 3.96 (H5′, $^2J_{5'5''}$ = 12.4 Hz), 3.74 (H5″) ppm.

proton−proton torsion angles from the lowest energy conformer of βC (**3**) at the HF/3-21G level is as large as 6.8 Hz, which shows that the E_5 conformer is not predominant in solution at 298 K (Table 3).

In further elaboration of conformational equilibria of **1**−**10**, we have assumed a two-state equilibrium which is supported by the small HF/3-21G energy difference between the two minima (see Table 3 and Figure 4). The conformational analysis of experimental $^3J_{HH}$ in **1**−**10** boils down to finding puckering parameters of the two conformers and mole fractions at each temperature that best fit our experimental $^3J_{HH}$ data set (eq 6). To reduce the number of parameters to be extracted from the experimental couplings, the geometry of the minor conformer in **1**−**5** was kept fixed during the optimization procedure to P_2 = 109.0°, Q = 42.4°, and Θ = −45.0°, which is close to $^6H_5$ canonical form (see the Experimental Section for details). The geometries of the major conformers in **1**−**5** were allowed to be optimized freely as well as the populations at all temperatures and conditions at which experimental $^3J_{HH}$ data were provided. The results are presented in Table 4. The variation in the pyranosyl puckering of the major conformers is very small among β- and α-nucleosides, which indicates that the nature of the nucleobase has a minor (if any) influence on the geometry of the major conformer in solution. The nature of purine *vs* pyrimidine moiety has however a great influence on the drive of the conformational equilibrium in **1**−**10**. The least-squares optimization procedure in which the starting geometry of major conformer of **1**−**5** was systematically varied gave the best fit with the root-mean-square error below 0.2 Hz (Table 4). The largest individual discrepancy in $^3J_{HH}$ was below 0.2 Hz for couplings along Csp^3-Csp^3 and below 0.4 Hz for couplings along Csp^2-Csp^3, which is well within the precision of the corresponding Karplus equations. Perusal of data in Table 4 shows that the pyranosyl puckering of the major conformers in β-anomers **1**−**5**, which was freely optimized, is intermediate between the ^5E and $^5S_4$ canonical forms. The conformational ranges for the major and the minor conformers involved in the two-state equilibrium of **1**−**10**, which show slightly worse agreement with the set of experimental $^3J_{HH}$ than the best fit, are given in the Experimental Section. It should be noted that the minor conformer is only populated by ca. 5% for **1** and **2** and ca. 20% for **3**−**5** at 278 K and therefore cannot be defined with high precision through the analysis of experimental coupling constants. For the α-anomers **6**−**10**, the experimental values for $^3J_{1'2'}$ were excluded from the least-squares optimization because the Karplus equation by Garbisch[17] cannot account for the coupling constants below 2.6 Hz. Results of the conformational analysis of the α-anomers **6**−**10** are presented

Table 3. Comparison of the Puckering Coordinates and the Corresponding Vicinal Proton−Proton Coupling Constants for βA (**1**), βG (**2**), and βC (**3**) Based on X-ray Crystal Structures, Two Lowest HF/3-21G Energy Conformers, and Geometries Obtained with Single-State Analysis of Experimental $^3J_{HH}$ at 298 K

		ring puckering							
		spherical coords.[a]				calculated coupling constants[b]			
compd	X-ray/E_{rel}/NMR	P_2	Q	Θ	form	$J_{1'2'}$ (ΔJ)	$J_{3'4'}$ (ΔJ)	$J_{4'5'}$ (ΔJ)	$J_{4'5''}$ (ΔJ)
βA (**1**)	X-ray[c]	290.9	42.7	49.9	$^5H_6$	3.8 (0.5)	4.6 (−0.5)	3.0 (0.4)	1.2 (−1.0)
	0.0[d]	291.2	46.3	47.4	$^5H_6$	4.1 (0.8)	4.9 (−0.2)	2.0 (−0.6)	1.8 (−0.4)
	+2.2[d]	109.0	44.2	−47.3	$^6H_5$	3.4 (0.1)	2.8 (−2.3)	6.9 (−4.3)	10.2 (8.0)
	single st.[e]	273.1	39.5	45.9	^5E	3.9 (0.6)	5.2 (0.1)	2.2 (−0.4)	1.4 (−0.8)
βG (**2**)	X-ray[c]	313.6	43.0	51.1	$E_6/^5S_6$	4.6 (1.3)	3.5 (−1.7)	5.8 (3.3)	0.7 (−1.1)
	0.0[d]	291.7	46.7	47.5	$^5H_6$	4.1 (0.8)	4.9 (−0.3)	2.0 (−0.5)	1.8 (0.0)
	+8.0[d]	109.1	44.2	−47.3	$^6H_5$	3.4 (0.1)	2.8 (−2.4)	6.8 (4.3)	10.2 (8.4)
	single st.[e]	263.2	38.0	52.2	^5E	3.5 (0.2)	5.3 (0.1)	2.3 (−0.2)	1.4 (−0.4)
βC (**3**)	X-ray[c]	113.9	45.5	−44.7	$^6H_5$	3.0 (0.0)	2.7 (−1.7)	5.9 (2.6)	10.7 (7.2)
	0.0[d]	107.3	44.8	−46.9	E_5	3.5 (0.5)	2.7 (−1.7)	6.6 (3.3)	10.3 (6.8)
	+3.5[d]	277.4	43.7	52.0	^5E	3.7 (0.7)	5.1 (0.7)	1.9 (−1.4)	1.9 (−1.6)
	single st.[e]	279.9	40.1	40.9	^5E	4.3 (1.3)	5.2 (0.8)	2.3 (−1.0)	1.4 (−2.1)

[a] P_2, Q, and Θ are given in degrees. [b] $^3J_{1'2'}$ and $^3J_{3'4'}$ have been calculated by the use of three-parameter Karplus equation,[17b] whereas $^3J_{4'5'}$ and $^3J_{4'5''}$ have been calculated by the generalized Karplus equation (eq 1).[16a] ΔJ is defined as $J^{calcd} - J^{expt}$. [c] Data from ref 15a. Note that each of the nucleosides **1**−**3** crystallizes with two structures in the unit cell. The values for P_2, Q, and Θ for one of them are given in the table. The other structure exhibits very similar puckering coordinates: $P_2 = 296.7°$, $Q = 43.7°$, and $\Theta = 46.9°$ for βA (**1**), $P_2 = 316.1°$, $Q = 41.7°$, and $\Theta = 51.0°$ for βG (**2**), and $P_2 = 111.0°$, $Q = 46.3°$, and $\Theta = -48.4°$ for βC (**3**). The orientation of the nucleobase across the glycosyl bond in **1**−**3** is *anti/high anti* relative to the pyranosyl moiety: χ[O6′−C1′−N9/1−C4/2] = 275° and 303° in βA (**1**), $\chi = 281°$ and 283° in βG (**2**), and $\chi = 218°$ and 251° in βC (**3**). [d] The lowest energy conformers which have been arbitrarily assigned the relative energy (in kJ mol^{-1}) of 0.0 are characterized by HF/3-21 energy of −802.52589 hartrees for βA (**1**), −876.99010 hartrees for βG (**2**), and −731.04383 hartrees for βC (**3**). [e] The experimental coupling constants at 298 K were analyzed with the iterative procedure of program PYRLW in terms of a single-state conformation. The P_2, Q, and Θ parameters of the assumed single conformer were changed in order to find the best fit between experimental and back-calculated $^3J_{HH}$.

in Table 4. Our analysis has shown that αA (**6**) and αG (**7**) are involved in an unbiased $^6H_5 \rightleftarrows {}^5E/{}^5H_6$ conformational equilibria (Table 4). The conformational equilibrium of α-anomers **8**−**10** show a bias toward the ^5E conformation (ca. 75% at 278 K, Table 4). The largest individual difference between the experimental and the calculated $^3J_{HH}$ values after the least-squares optimization procedure in **6**−**10** was below 0.2 Hz for couplings along C4′−C5′ and below 0.5 Hz for couplings along C3′−C4′ bond with the overall root-mean-square error below 0.2 Hz (Table 4).

Populations of puckered $^6H_5$ and $^5E/{}^5S_4$ pyranosyl conformers at various temperatures in the range from 278 to 358 K were used to construct van't Hoff plots to determine the enthalpy ($\Delta H°$) and the entropy ($\Delta S°$) of the $^6H_5 \rightleftarrows {}^5E/{}^5S_4$ conformational equilibria of **1**−**10** in aqueous solution (Figure 5). Straight lines were obtained, which support the model of a two-state conformational equilibrium for the pyranose rings of **1**−**10**. We note that the Pearson correlation coefficients between $\ln(x_{5E}/x_{6H5})$ and $1/T$ were >0.96 for all compounds, except for αA (**6**) and αG (**7**) which have slopes of the van't Hoff curves close to zero and therefore the Pearson correlation coefficients are close to zero. The values for enthalpies and entropies, obtained from the slope and intercept of van't Hoff curves, respectively, for **1**−**10** are given in Table 5.

Discussion

From the results of the conformational analysis of $^3J_{HH}$ presented in Tables 4 and 5, it is evident that β-anomers **1**−**5** have highly similar conformational properties with respect to the pyranose rings. In all β-anomers, we have found in D_2O a pronounced preference for the conformation which is intermediate between the ^5E envelope and $^5S_4$ screw-boat forms. In **1**−**5**, $\Delta H°$ contributions to $\Delta G°$ drive the $^6H_5 \rightleftarrows {}^5E/{}^5S_4$ equilibrium toward $^5E/{}^5S_4$ conformation and are ca. two times stronger than entropy contributions at 298 K (Table 5). β-Purine nucleosides **1** and **2** show in D_2O larger conformational bias toward the $^5E/{}^5S_4$ conformation than their pyrimidine counterparts **3**−**5**. α-Purine nucleosides αA (**6**) and αG (**7**) are in D_2O involved in ca. 1:1 conformational equilibrium with $\Delta G°$ values close to zero. Their α-pyrimidine counterparts **8**−**10** show at 298 K, however, a preference for the ^5E conformation of ca. 75% which is reflected in negative $\Delta G°$ values between −2.3 and −2.8 kJ mol^{-1} (Table 5).

A tentative explanation of our findings is derived on the basis of the structures of the $^6H_5$ and $^5E/{}^5S_4$ conformers shown in Figure 6. The conformational equilibrium of pyranosyl residue in **1**−**10** is driven by the exocyclic substituents, which have the 4′-OH group as a common feature to all compounds and a nucleobase in either the β- or α-configuration. We have considered five principal stereoelectronic effects which control the $^6H_5 \rightleftarrows {}^5E/{}^5S_4$ equilibrium: (1) the gauche effect (GE) of [O6′−C5′−C4′−O4′] fragment, (2) the anomeric effect (AE) which is nucleobase dependent, (3) the interaction of π system across C2′−C3′ with the σ^* orbital of C4′−O4′ bond ($\pi \rightarrow \sigma^*_{C4'-O4'}$), (4) the interaction of π system across C2′−C3′ with the σ^* orbital of the glycosyl bond ($\pi \rightarrow \sigma^*_{C1'-N9/1}$), and (5) the steric preferences (SE) of the substituents for equatorial orientation, the heterocyclic aglycon in particular. Model building[22] of β-anomers shows that in the major conformer of **1**−**5**, which is intermediate between the ^5E and $^5S_4$ canonical forms, both the nucleobase and 4′-OH group are in axial orientation (Figure 6A). The conversion to the $^6H_5$ conformation results in the experimentally undesirable equatorial orientation of both the base and 4′-OH. Clearly, the anomeric and gauche effects are cooperative and both drive the $^6H_5 \rightleftarrows {}^5E/{}^5S_4$ equilibrium toward the $^5E/{}^5S_4$ conformer (Figure 6A). In addition, both $\pi \rightarrow \sigma^*_{C4'-O4'}$ and $\pi \rightarrow \sigma^*_{C1'-N9/1}$ interactions are optimal in the $^5E/{}^5S_4$ form. Repulsive steric interactions of the nucleobase with the axial hydrogen at C5′ and other substituents drive the conformational equilibrium toward the $^6H_5$ conformation in which the nucleobase is in equatorial orientation (Figure 6A).

For α-anomers **6**−**10**, the interplay of stereoelectronic effects is slightly altered. Model building[22] of **6**−**10** shows that the

(22) Insight II, Molecular Modeling System, version 95.0; Biosym/MSI: San Diego, CA, 1995.

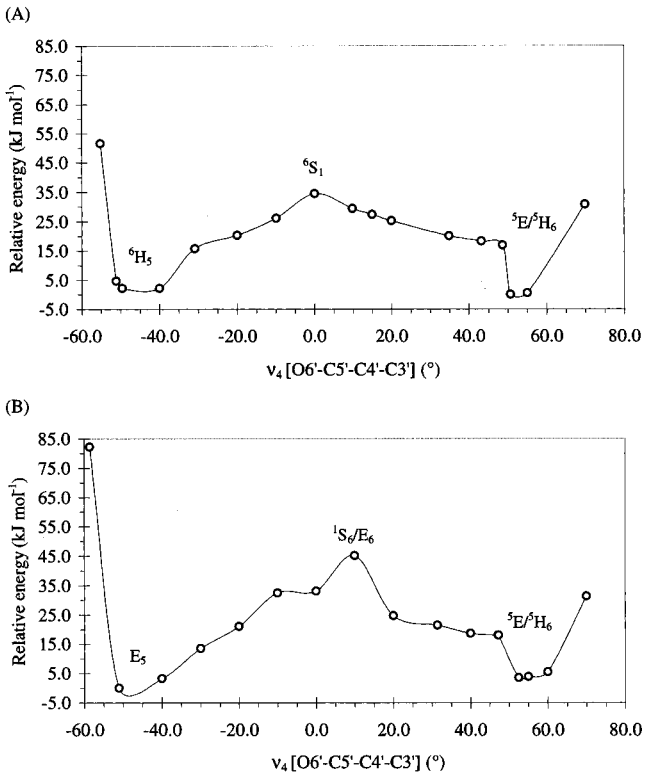

Figure 4. Plot of the relative Hartree−Fock energy (in kJ mol^{-1}) as a function of the endocyclic torsion angle ν_4 [O6′−C5′−C4′−C3′] for βA (**1**) in panel A and βC (**3**) in panel B. The profiles were obtained through optimization at the HF/3-21G level by keeping ν_4 constrained at distinct values, while all other degrees of freedom were freely optimized. The conformers in the energy minima are the result of completely free optimization. The calculations on both βA (**1**) and βC (**3**) showed two energy minima which are presented in Table 3. The lowest energy minimum for βA (**1**) is found at ν_4= 50.7° (panel A) and corresponds to the $^5H_6$ canonical form. The second lowest energy minimum for βA (**1**) is found at ν_4= −49.6° ($^6H_5$ canonical form) and has relative energy of 2.2 kJ mol^{-1} above the global minimum. The barrier of 34.5 kJ mol^{-1} between the two energy minima for βA (**1**) is found at ν_4 = 0.0°. The lowest energy minimum for βC (**3**) shown in panel B appears at ν_4 = −51.0° and corresponds to the E_5 canonical form (Table 3). The second lowest energy minimum for βC (**3**) is found at ν_4= 52.5° (^{5}E canonical form) and is characterized by E_{rel} = 3.5 kJ mol^{-1} above the lowest minimum. The barrier of 45.2 kJ mol^{-1} between the two energy minima for βC (**3**) is found at ν_4 = 10.0°.

4′-OH is in axial orientation in the ^{5}E conformer, whereas the nucleobase is in the equatorial orientation (Figure 6B). This means that the gauche effect of the [O6′−C5′−C4′−O4′] fragment and $\pi \rightarrow \sigma^*_{C4'-O4'}$ interactions both prefer the ^{5}E conformation, whereas anomeric effect and $\pi \rightarrow \sigma^*_{C1'-N9/1}$ interactions drive the equilibrium toward the $^6H_5$ conformation. Additionally, the steric bulk of the nucleobase on the sterically crowded α side of the sugar moiety drives the $^6H_5 \rightleftarrows {}^5$E equilibrium in **6**−**10** toward the ^{5}E conformation (Figure 6B). We can therefore write the relative contributions to the drive of two-state conformational equilibrium in **1**−**10** in the form of two separate equations for β- (eq 7) and α- (eq 8) anomers.

$$\beta\text{-anomers: } \Delta H^\circ \text{ or } \Delta G^\circ \text{ (kJ mol}^{-1}) \equiv -\text{GE} - \text{AE} - (\pi \rightarrow \sigma^*_{C4'-O4'}) - (\pi \rightarrow \sigma^*_{C1'-N9/1}) + \text{SE}^\beta \quad (7)$$

$$\alpha\text{-anomers: } \Delta H^\circ \text{ or } \Delta G^\circ \text{ (kJ mol}^{-1}) \equiv -\text{GE} + \text{AE} - (\pi \rightarrow \sigma^*_{C4'-O4'}) + (\pi \rightarrow \sigma^*_{C1'-N9/1}) - \text{SE}^\alpha \quad (8)$$

The negative sign of terms in eqs 7 and 8 denotes a drive of the $^6H_5 \rightleftarrows {}^5E/{}^5S_4$ conformational equilibrium by a particular stereoelectronic effect toward the conformation which is intermediate between the ^{5}E and $^5S_4$ canonical forms, whereas a positive sign denotes a drive toward $^6H_5$ conformation. In order to dissect the experimental ΔH° values in **1**−**10** into the five postulated contributions, we have turned to the results of the evaluation of the individual gauche and anomeric effects in natural nucleosides.[2] The comparative analysis of ΔH° of the North ⇄ South pseudorotational equilibria in pentofuranosyl nucleosides[2] has shown that the strength of the gauche effect of the [O4′−C4′−C3′−O3′] fragment is 7.3 kJ mol^{-1}. Additionally, it has been shown[2] that the anomeric effect is nucleobase dependent and ΔH° values are 2.1 kJ mol^{-1} for adenine, 3.1 kJ mol^{-1} for guanine,[24] 5.2 kJ mol^{-1} for cytosine, 3.7 kJ mol^{-1} for thymine, and 4.5 kJ mol^{-1} for uracil. It should be noted that these estimates of the anomeric effect combine both the strength of $n_{O4'} \rightarrow \sigma^*_{C1'-N9/1}$ interaction and the inherent steric effect of the nucleobase. The comparison of the steric energies in the computer models of the North *vs* South conformers in β-pentofuranosyl nucleosides with the $^6H_5$ *vs* ^{5}E/$^5S_4$ puckered pyranosyl moieties in **1**−**5** suggests that the steric repulsions of the nucleobase with other substituents are comparable in the two sets of compounds. The subtraction of the gauche and anomeric effects from experimental ΔH° values in **1**−**10** enabled us to calculate (eqs 7 and 8) the resultant of the $\pi \rightarrow \sigma^*$ interactions in **1**−**10**. The results are presented in the form of bar graph in Figure 7 and show that there is a net drive toward the ^{5}E conformation in βA (−1.9 kJ mol^{-1}) and βG (−4.7 kJ mol^{-1}), whereas β-pyrimidine nucleosides are characterized with the resultant which drives the $^6H_5 \rightleftarrows {}^5E/{}^5S_4$ equilibrium toward the $^6H_5$ conformation (6.6 kJ mol^{-1} for βC, 3.5 kJ mol^{-1} for βT, and 4.5 kJ mol^{-1} for βU) (Figure 7A). In all β-anomers **1**−**5**, the $\pi \rightarrow \sigma^*_{C4'-O4'}$ interactions are a constant force which drives the equilibrium toward the $^5E/^5S_4$ conformations cooperatively with $\pi \rightarrow \sigma^*_{C1'-N9/1}$ interactions (see Figure 6A). At the moment, we are not able to distinguish between the individual contributions of the two cooperative $\pi \rightarrow \sigma^*$ effects. Nevertheless, the bar graphs in Figure 7A show that the sum of the two effects clearly drives the conformational equilibrium in **1**−**5** toward the $^5E/^5S_4$ conformation more efficiently in β-purines than in β-pyrimidines. This indicates that $\pi \rightarrow \sigma^*_{C1'-N9/1}$ interactions are more efficient when the nitrogen atom is part of the electron-rich imidazole moiety of purine than part of the electron-deficient pyrimidine and increase in the following order: cytosine < uracil < thymine < adenine < guanine.

The subtraction of the strength of the gauche and anomeric effects from the experimental ΔH° values in **6**−**10** according to eq 8 has shown that there is a net drive toward the $^6H_5$ conformation in αA (5.1 kJ mol^{-1}) and αG (4.4 kJ mol^{-1}). Similar dissection of the individual contributions to ΔH° in α-nucleosides pyrimidine shows that the resultant of $\pi \rightarrow \sigma^*_{C1'-N9/1}$ and $\pi \rightarrow \sigma^*_{C4'-O4'}$ interactions drives the $^6H_5 \rightleftarrows {}^5$E equilibrium in **8**−**10** toward the ^{5}E conformer in αC (−2.9 kJ mol^{-1}) and toward the $^6H_5$ conformation in αT (2.2 kJ mol^{-1}) and αU (1.2 kJ mol^{-1}). It is clear from Figure 6B that the $\pi \rightarrow \sigma^*_{C1'-N9/1}$ and $\pi \rightarrow \sigma^*_{C4'-O4'}$ interactions oppose each other in the drive of the $^6H_5 \rightleftarrows {}^5$E equilibrium in **6**−**10**. The $\pi \rightarrow \sigma^*_{C4'-O4'}$ interactions are a constant force in all α-anomers **6**−**10**, which enables us to qualitatively scale the strengths of $\pi \rightarrow \sigma^*_{C1'-N9/1}$ interactions in purine and pyrimidine nucleosides. In α-purines the driving force toward the $^6H_5$ conformation is larger than that in the α-pyrimidines, which suggests that $\pi \rightarrow \sigma^*_{C1'-N9/1}$ interactions are stronger when the nitrogen atom is part of the electron-rich system than when it is part of the electron-deficient heterocyclic system. It should be noted

Table 4. Conformational Equilibria of the Pentopyranosyl Moieties of **1**−**10** in Aqueous Solution

	major conformer[a]			population (% $^5E/^5S_4$)		error analysis[b] (Hz)				
compd	P_2	Q	Θ	278 K	358 K	$^3J_{4'5'}$	$^3J_{4'5''}$	$^3J_{1'2'}$	$^3J_{3'4'}$	rms
βA (**1**)	257.3	36.9	55.3	94.4	84.8	0.2	<0.1	0.2	0.1	0.07
βG (**2**)	257.0	36.9	55.4	96.5	87.4	0.1	<0.1	0.1	<0.1	0.06
βC (**3**)	250.5	36.3	59.4	78.9	67.3	0.2	0.1	0.3	0.4	0.23
βT (**4**)	252.9	36.3	58.4	81.3	67.2	0.2	<0.1	0.4	0.4	0.20
βU (**5**)	253.1	36.1	58.2	83.2	71.2	0.1	<0.1	0.3	0.3	0.16
αA (**6**)	293.6	43.5	47.5	53.9	53.6	0.1	<0.1		0.1	0.08
αG (**7**)	292.4	42.1	48.3	46.6	46.6	0.2	<0.1		0.5	0.19
αC (**8**)	271.4	37.2	49.8	77.9	72.7	<0.1	<0.1		<0.1	0.03
αT (**9**)	284.0	40.1	45.7	75.4	72.8	<0.1	<0.1		<0.1	0.04
αU (**10**)	284.1	40.1	45.6	73.1	69.8	<0.1	<0.1		<0.1	0.03

[a] The puckering parameters P_2, Q, and Θ are given in degrees. The geometry of the minor conformer was kept fixed at $P_2 = 109.0°$, $Q = 42.4°$, and $\Theta = -45.0°$, which is close to the $^6H_5$ canonical form. [b] The largest absolute discrepancy between J^{expt} and J^{calcd} at five temperatures in D_2O is tabulated. For α-isomers **6**−**10**, $^3J_{1'2'}$ was not used in the PYRLW analysis because Garbisch equation[17] cannot account for the experimental coupling constants below 2.6 Hz.

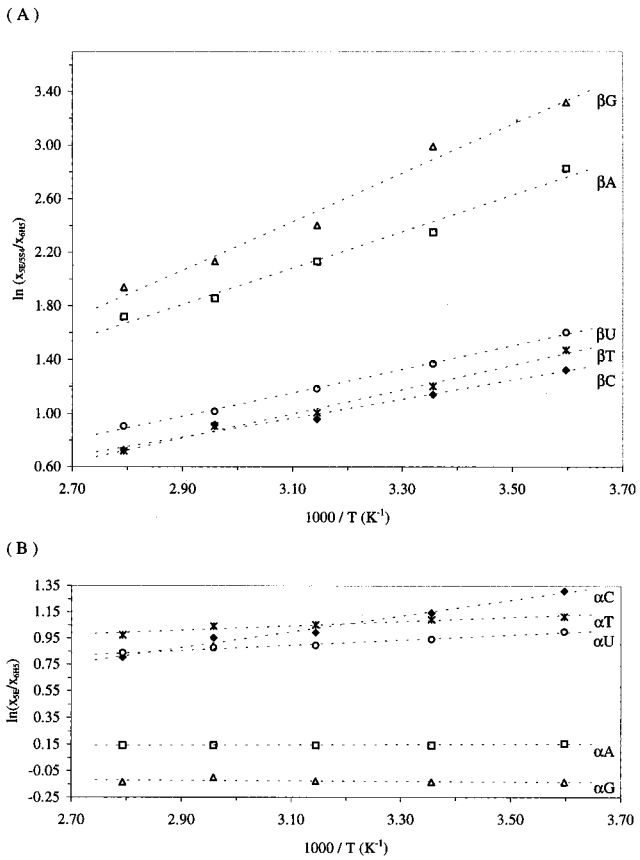

Figure 5. Van't Hoff plots of $\ln(x_{5E}/x_{6H5})$ as a function of reciprocal of temperature for β nucleosides **1**−**5** (panel A) and for α nucleosides **6**−**10** (panel B). Mole fractions of the ^5E and $^6H_5$ conformers were determined through the analysis of $^3J_{HH}$ measured at five temperatures ranging from 278 to 358 K with the PYRLW program. From the slope and the intercept with ordinate of the straight lines, $\Delta H°$ and $\Delta S°$ were calculated according to the relation: $\ln(x_{5E}/x_{6H5}) = -(\Delta H°/R)(1000/T) + \Delta S°/R$. The Pearson correlation coefficients (R) are 0.990 for βA (**1**), 0.990 for βG (**2**), 0.987 for βC (**3**), 0.995 for βT (**4**), 0.999 for βU (**5**), 0.751 for αA (**6**), −0.045 for αG (**7**), 0.990 for αC (**8**), 0.959 for αT (**9**), and 0.992 for αU (**10**).

however, that the steric repulsions are expected to be larger on the α side compared to β side of the pyranose ring in **1**−**10**. A larger drive toward the ^5E conformation in α-pyrimidine compared to that in α-purine nucleosides might indicate that the steric bulk of the former is larger and therefore forcing the base into the equatorial orientation (*i.e.*, ^5E conformer) more effectively. We are however at present not able to distinguish between the individual contributions of the steric effects, $\pi \rightarrow \sigma^*_{C1'-N9/1}$ and $\pi \rightarrow \sigma^*_{C4'-O4'}$ interactions which drive the $^6H_5 \rightleftarrows {}^5E$ equilibrium in **6**−**10**.

The results of the conformational analysis of $^3J_{HH}$ in **1**−**10** in DMSO suggest a strong solvent dependence on stereoelectronic effects which drive the conformational equilibrium in **1**−**10** (Table 5). β-Purine nucleosides **1** and **2** show in DMSO at 298 K high conformational preference of ca. 73% toward the conformation intermediate between the ^5E and $^5S_4$ canonical forms (Table 5). Note that the conformational bias in **1** and **2** has been reduced by ca. 20% units when D_2O has been replaced by DMSO. Their pyrimidine counterparts (**3**−**5**) exhibit in DMSO at 298 K a slight preference of ca. 60% for the $^6H_5$ canonical form (Table 5). The approximately 75% conformational preference of pyranosyl moiety in **3**−**5** for the conformation that is intermediate between the ^5E and $^5S_4$ forms in D_2O has been, in DMSO, reduced by 34 to 41% units and actually inverted in favor of the $^6H_5$ form. The α-purine nucleosides αA (**6**) and αG (**7**) are, in DMSO, involved in approximately 70:30 conformational equilibrium between the $^6H_5$ and ^5E forms (Table 5). Their α-pyrimidine counterparts **8**−**10** show, however, a preference of 63−70% for the ^5E conformation (Table 5). Note that the conformational equilibrium in **6** and **7** has been shifted by ca. 22% units when D_2O has been replaced by DMSO. The comparison of the conformational preferences of pyranosyl moieties of **8**−**10** in D_2O and in DMSO shows that the preference for the ^5E conformation has been reduced by 5−11% units due to the change of solvent (Table 5).

Conclusions

Conformational characteristics of pyranosyl moiety in D-*glycero*-pent-2′-enopyranosyl nucleosides **1**−**10** have been studied by ^1H NMR spectroscopy and compared with the results of X-ray crystallography and *ab initio* calculations. The experimental $^3J_{HH}$ coupling constants acquired in D_2O and in DMSO-d_6 were interpreted in terms of a two-state conformational equilibrium between the $^6H_5$ conformation and the conformation which is intermediate between the ^5E and $^5S_4$ canonical forms. The β nucleosides **1**−**5** adopt predominantly the $^5E/^5S_4$ conformation where the nucleobase is placed in the axial orientation. There is a noticeable difference in the conformational preferences between β-purines **1** and **2** (approximately 95% at 298 K in D_2O) and β-pyrimidine analogues **3**−**5** (approximately 80%). The high conformational bias toward the $^5E/^5S_4$ conformers in **1**−**5** is the result of cooperative drive of the gauche effect of the [O6′−C5′−C4′−O4′] fragment, the nucleobase-dependent anomeric effect, and the resultant of $\pi \rightarrow \sigma^*_{C4'-O4'}$ and $\pi \rightarrow \sigma^*_{C1'-N9/1}$ interactions which are opposed by the steric preference of the nucleobase for the $^6H_5$ conformation. The sugar moiety

Table 5. Thermodynamic Parameters for the $^6H_5 \rightleftarrows {}^5E/{}^5S_4$ Conformational Equilibrium in **1**−**10** in D_2O and DMSO-d_6

	D_2O					DMSO-d_6	
compd	$\Delta H°$	$\Delta S°$	$-T\Delta S°$ (298 K)	$\Delta G°$ (298 K)	$\%{}^5E/{}^5S_4$ (298 K)	$\Delta G°$ (298 K)	$\%{}^5E/{}^5S_4$ (298 K)
βA (**1**)	−11.3	−17.8	5.3	−6.0	91.8	−2.4	72.5
βG (**2**)	−15.1	−26.5	7.9	−7.2	94.8	−2.7	74.8
βC (**3**)	−5.9	−10.3	3.1	−2.8	75.6	0.8	42.0
βT (**4**)	−7.5	−15.0	4.5	−3.0	77.0	1.4	36.2
βU (**5**)	−7.3	−12.9	3.8	−3.5	80.4	0.9	41.0
αA (**6**)	−0.1	0.9	−0.3	−0.4	54.0	2.1	30.0
αG (**7**)	0.2	−0.6	0.2	0.4	46.0	2.6	25.9
αC (**8**)	−5.0	−7.3	2.2	−2.8	75.6	−1.6	65.6
αT (**9**)	−1.4	4.5	−1.3	−2.7	74.8	−2.1	70.0
αU (**10**)	−1.6	2.4	−0.7	−2.3	71.7	−1.3	62.8

[a] $\Delta H°$ and $\Delta G°$ are given in kJ mol^{-1}; $\Delta S°$ is in J mol^{-1} K^{-1}. A negative sign for $\Delta H°$, $-T\Delta S°$, and $\Delta G°$ denotes a drive of the conformational equilibrium toward the $^5E/^5S_4$ canonical form, whereas a positive sign denotes a drive toward the $^6H_5$ from. Error estimates for $\Delta H°$ and $\Delta S°$ are ±0.3 kJ mol^{-1} and ±2.0 J mol^{-1} K^{-1}, respectively.

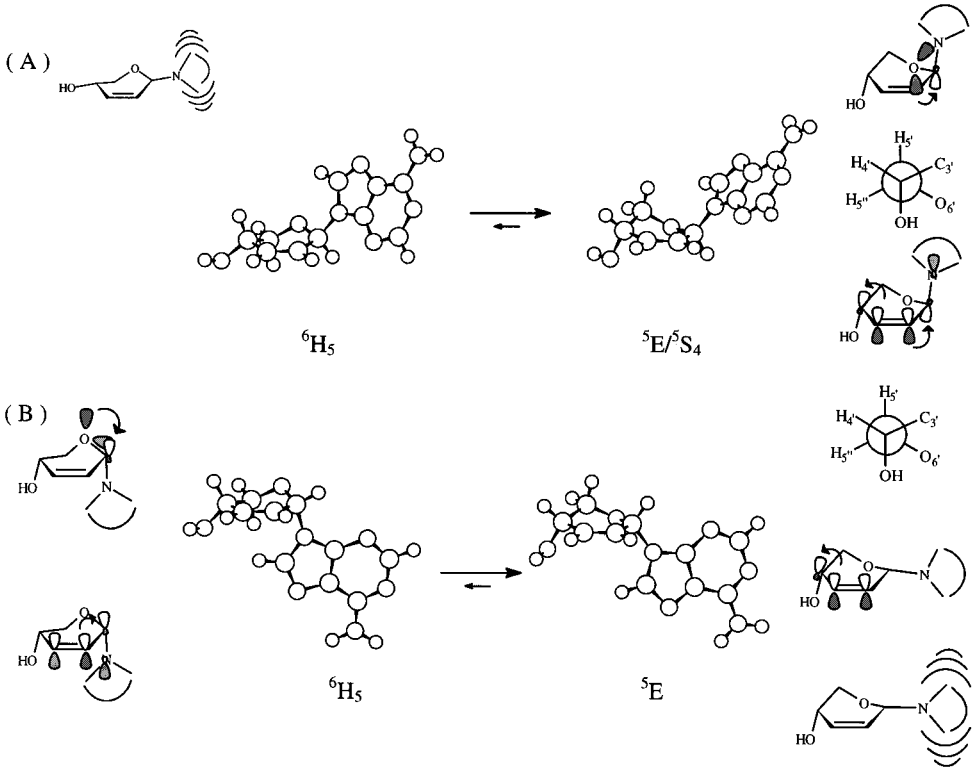

Figure 6. Stereochemical relationships of the 4′-OH group and the nucleobase with respect to O6′ and the C2′−C3′ double bond between conformers involved in a two-state equilibrium of **1**−**10** in β nucleosides (panel A) and in α nucleosides (panel B). Note that anomeric effect ($n_{O6'} \rightarrow \sigma^*_{C1'-N9/1}$ interaction) drives the conformational equilibrium toward the $^5E/^5S_4$ conformers in β-anomers (panel A) and toward the $^6H_5$ conformers in α-anomers (panel B). The gauche effect of the [O6′−C5′−C4′−O4′] fragment and the $\pi \rightarrow \sigma^*_{C4'-O4'}$ interaction drive the equilibrium toward the $^5E/^5S_4$ conformers in both β- (panel A) and α-anomers (panel B). The $\pi \rightarrow \sigma^*_{C1'-N9/1}$ interaction is optimal in the $^5E/^5S_4$ conformers in the β-anomers (panel A) and in the $^6H_5$ conformers in the α-anomers (panel B). The steric bulk of the nucleobase results in the preference for the $^6H_5$ conformers in the β-anomers (panel A) and the ^5E conformers in the α-anomers (panel B).

in α-purine nucleosides **6** and **7** in aqueous solution is involved in an unbiased two-state conformational equilibrium. On the other hand, the α-pyrimidine nucleosides **8**−**10** show a conformational bias of ca. 75% toward the ^5E canonical form. Thermodynamic data on the two-state conformational equilibrium of pyranosyl moiety in **1**−**10** suggests that $\pi \rightarrow \sigma^*_{C1'-N9/1}$ interaction greatly depends on the nature of the heterocyclic aglycon. It is much stronger when the nitrogen atom is part of the electron-rich imidazole moiety of a purine residue than when it is in the electron-deficient pyrimidine. The strength of the $\pi \rightarrow \sigma^*_{C1'-N9/1}$ interaction increases in the following order: cytosine < uracil < thymine < adenine < guanine.

Experimental Section

NMR Spectroscopy. ^{1}H NMR spectra were recorded at 299.942 MHz on Varian UnityPlus NMR spectrometer at the National NMR Center of Slovenia. D_2O (99.9% deuterium) or DMSO-d_6 (99.9% deuterium) were used as solvents. The sample temperature was controlled to approximately ±0.5 K. Sample concentration was 10 mM, except for **2** which was 1.5 mM in D_2O. All measurements were performed under identical spectral and processing conditions: 2800 Hz sweep width, 32K time domain, zero-filling to 64K, and slight apodization to give resolution enhancement. Spectra were simulated with a standard computer simulation algorithm, which is integrated into Varian software (VNMR version 5.1A), in order to obtain accurate J coupling data and chemical shifts. One-dimensional NOE experiments were run with 5 s irradiation time and with saturation of individual lines within the multiplet. NOE difference spectra were obtained by internal subtraction of on- and off-resonance spectra.

Analysis of $^3J_{HH}$. The conformational analysis of pyranosyl moiety in **1**−**10** has been performed with the use of our computer program PYRLW which finds the best fit between experimental and calculated $^3J_{HH}$. The program PYRLW has been written in FORTRAN and run

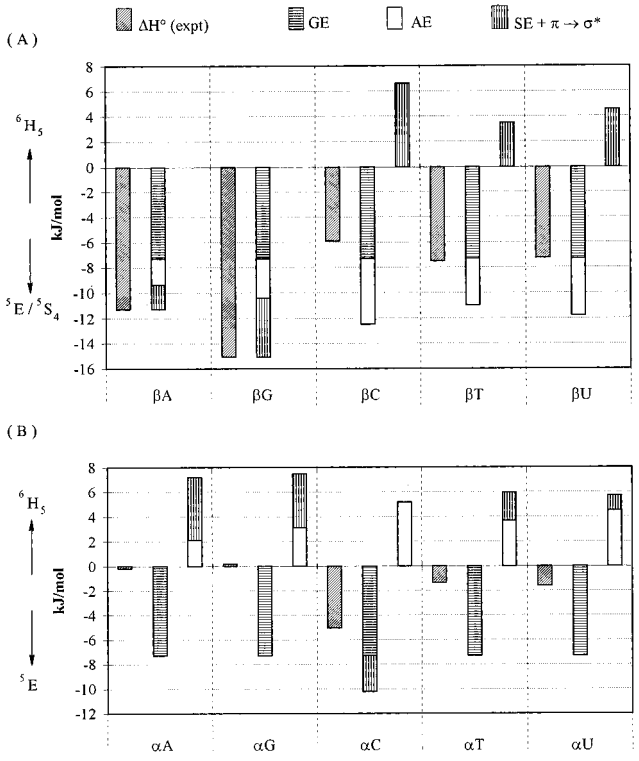

Figure 7. Relative contributions of the effects (in kJ mol^{-1}) that compete in the drive of the $^6H_5 \rightleftarrows {}^5E/{}^5S_4$ equilibrium in β-anomers **1**−**5** (panel A) and in α-anomers **6**−**10** (panel B). The experimental $\Delta H°$ values are represented by the bars on the left side (bars shaded with tilted lines). The conformational equilibrium is driven by the combination of the gauche effect (GE) of [O6′−C5′−C4′−O4′] fragment (bars with horizontal lines), the anomeric effect (AE) of the nucleobase (white bars), and the combination of the $\pi \rightarrow \sigma^*_{C4'-O4'}$ interaction, the $\pi \rightarrow \sigma^*_{C1'-N9/1}$ interaction, and the steric preferences of the nucleobase for equatorial orientation (bars with vertical lines). The gauche effect drives the $^6H_5 \rightleftarrows {}^5E/{}^5S_4$ equilibrium toward the $^5E/{}^5S_4$ conformation in both β- (panel A) and α-anomers (panel B). The anomeric effect drives the conformational equilibrium toward $^5E/{}^5S_4$ conformation in β anomers (panel A) and toward the $^6H_5$ conformation in α-anomers (panel B). See the text for the interpretation of the resultant of the competing effect of the $\pi \rightarrow \sigma^*_{C4'-O4'}$ interaction, the $\pi \rightarrow \sigma^*_{C1'-N9/1}$ interaction, and the steric preferences on the drive of the $^6H_5 \rightleftarrows {}^5E/{}^5S_4$ equilibrium in **1**−**10**.

on SG Indigo2 computer. The input consists of the parameters P_1−P_6 (eq 1), the λ electronegativities of the four substituents (along C4′−C5′ bond), *A* and *B* parameters, the experimental $^3J_{HH}$, and the initial guesses of the geometries of the starting conformers and their respective populations. The following λ electronegativity values[16a] have been used: 0.0 for H, 1.26 for O6′, 1.25 for OH, and 0.5 for C3′. The discrepancy between experimental and calculated $^3J_{HH}$ has been monitored through the calculation of root-mean-square $= [{}^1/_M\sum_{i=1}^{M}[J_i^{expt} - J_i^{calcd}(P_2^I, \Phi_2^I, \Phi_3^I, P_2^{II}, \Phi_2^{II}, \Phi_3^{II}, x^{II})]^2]^{1/2}$. As one of the conformers is populated by less than 5−25% in **1**−**5** and **8**−**10**, we have constrained its geometry during the iteration procedure. The starting puckering parameters of the minor conformers have been fixed to $P_2 = 107°$, $\Phi_2 = 33°$, and $\Phi_3 = -31°$, which corresponds to the geometry of the lowest energy conformer from HF/3-21G *ab initio* optimization of βC (**3**). To find the global minimum, we systematically varied input parameters for the major conformer in the following way: Φ_2 was set to 30° or 50°, P_2 was set to 0°, 90°, 180°, or 270°, and Φ_3 was independently set to −30°, 0°, or 30°. The results of these 24 pilot analyses of experimental $^3J_{HH}$ have shown that acceptable fit (maximum individual ΔJ < 0.8 Hz and root-mean-square error < 0.5 Hz) between experimental and calculated $^3J_{HH}$ has been found only when the starting puckering parameters of the major conformers have been set to $\Phi_2 = 30°$, $P_2 = 180°$ or 270°, and $\Phi_3 = 0°$ or 30°. After finding the geometry of the major conformer (see below) which gives the low root-mean-square error, we have constrained the major conformer to the optimized geometry and varied P_2, Φ_2, and Φ_3 of the minor conformer to improve the agreement between J^{expt} and J^{calcd}. The smallest root-mean-square error and the lowest difference between J^{expt} and J^{calcd} were obtained with $P_2 = 109°$, $\Phi_2 = 30°$, and $\Phi_3 = -30°$ as the minor conformer, which were in further optimizations of **1**−**10** constrained to assume fixed value when the geometry of the major conformer was optimized.

In our additional analysis of $^3J_{HH}$ in **1**−**10**, we wanted to determine (1) the conformational range of the major conformer, when minor is constrained to the $^6H_5$ canonical form, and (2) the reverse, the conformational range of the minor conformer when major is kept fixed. We have found that the conformational equilibria in **1**−**10** are defined by [40° < P_2 < 150°, 30° < Φ_2 < 50°, −50° < Φ_3 < −5°, 30° < Q < 70°, −80° < Θ < −45°] $\rightleftarrows$ [230° < P_2 < 275°, 27° < Φ_2 < 38°, 11° < Φ_3 < 27°, 39° < Q < 40°, 45° < Θ < 75°] for β-purine nucleosides **1** and **2**, [60° < P_2 < 150°, 30° < Φ_2 < 70°, −60° < Φ_3 < −20°, 36° < Q < 90°, −56° < Θ < −45°] $\rightleftarrows$ [230° < P_2 < 265°, 28° < Φ_2 < 39°, 10° < Φ_3 < 24°, 37° < Q < 41°, 50° < Θ < 77°] for β-pyrimidine nucleosides **3** to **5**, [85° < P_2 < 140°, 25° < Φ_2 < 35°, −35° < Φ_3 < −20°, 36° < Q < 50°, −56° < Θ < −44°] $\rightleftarrows$ [270° < P_2 < 295°, 29° < Φ_2 < 32°, 23° < Φ_3 < 29°, 37° < Q < 43°, 48° < Θ < 52°] for α-purine nucleosides **6** and **7**, and [50° < P_2 < 150°, 20° < Φ_2 < 50°, −50° < Φ_3 < −10°, 25° < Q < 70°, −70° < Θ < −45°] $\rightleftarrows$ [240° < P_2 < 290°, 28° < Φ_2 < 34°, 15° < Φ_3 < 30°, 37° < Q < 42°, 43° < Θ < 69°] for α-pyrimidine nucleosides **8**−**10**. The populations of the two conformers in the above sets of best fits between J^{expt} and J^{calcd} have at a particular temperature varied by ±2% units in **1** and **2**, by ±1.5% units in **3**−**5** and **8**−**10**, and by ±1% unit in **6** and **7**. The deviation between J^{expt} and J^{calcd} coupling constants in the above analyses was below 0.4 Hz for $^3J_{4'5'}$, $^3J_{4'5''}$, and $^3J_{3'4'}$ and below 0.7 Hz for $^3J_{1'2'}$ with an overall root-mean-square error below 0.4 Hz.

***Ab Initio* Calculations.** All calculations were performed with Gaussian 94 program[23] running on Silicon Graphics Indigo 2 (SGI-G94 revision D.1) or Indy (SGI-G94 revision C.3) with R4000 processor and Hewlett Packard (HP-PARisc-HPUX-G94 revision D.1) series 700 computers. For all of the compounds, all internal degrees of freedom were freely optimized at the HF/3-21G level except for the energy profiles shown in Figure 4, where ν_4 was kept fixed to scan the conformational space (typical CPU time was 10 h). Optimized values were used as input for the geometry optimizations at HF/6-31G(d,p) level (typical CPU time was 4 days). Stationary points were verified through vibrational frequency calculations.

Acknowledgment. We thank the Ministry of Science and Technology of the Republic of Slovenia for financial support. Financial aid from Krka Pharmaceutical and Chemical Works, Novo mesto, Slovenia is gratefully acknowledged. We also thank Prof. J. Chattopadhyaya, Department of Bioorganic Chemistry, Uppsala University, Sweden, for the generous offer of computer time.

JA963683K

(23) Gaussian 94; Frisch, M. J.; Trucks, G. W.; Schlegel, H. B.; Gill, P. M. W.; Johnson, B. G.; Robb, M. A.; Cheeseman, J. R.; Keith, T.; Petersson, G. A.; Montgomery, J. A.; Raghavachari, K.; Al-Laham, M. A.; Zakrzewski, V. G.; Ortiz, J. V.; Foresman, J. B.; Cioslowski, J.; Stefanov, B. B.; Nanayakkara, A.; Challacombe, M.; Peng, C. Y.; Ayala, P. Y.; Chen, W.; Wong, M. W.; Andres, J. L.; Replogle, E. S.; Gomperts, R.; Martin, R. L.; Fox, D. J.; Binkley, J. S.; Defrees, D. J.; Baker, J.; Stewart, J. P.; Head-Gordon, M.; Gonzalez, C.; Pople, J. A. Gaussian, Inc.: Pittsburgh, PA, 1995.

(24) The estimate for the strength of O−C−N anomeric effect of guanine is used for the N^2-isobutyrylguanine.